Terra Nova

doi: 10.1111/ter.12105

Influence of inherited topography on gravitational slope failure: three-dimensional numerical modelling of the La Clapière slope, Alpes-Maritimes, France

Thomas Bois, Emmanuel Tric and Thomas Lebourg

Université de Nice Sophia Antipolis, CNRS, IRD, Observatoire de la Cote d'Azur, Géoazur UMR 7329, 250 rue A. Einstein, Valbonne 06560, France

ABSTRACT

Gravitational slope failure involves rock slopes at various scales. Nowadays, it is accepted that different factors influence slope destabilization, including topography. In many cases, slope failure occurs between tributary valleys cutting the slope. In this study, we ask what influence tributary valleys have on slope failure. To tackle this question, we developed a 3-D numerical model of the La Clapière Slope and then examined a series of simplified 3-D models with different geometries of tributary valleys (spacing and depth). Our results show that: (1) whatever considered *in situ* stresses are, including the third dimension reduces the destabilization threshold compared with 2-D models; and (2) the spacing and the depth of tributary valleys influence slope failure. For shallow incisions, increasing the lateral spacing between tributary valleys does not affect failure localization but does increase slope damage (to a stable value from 2000 m). However, deeper incision does not affect slope damage but does contribute to failure localization. When the spacing is less than 1500 m, the part of the slope between tributary valleys is not involved in the failure process, but for spacings above 1500 m slope failure occurs between tributary valleys.

Terra Nova, 26, 354–362, 2014

Introduction

Slope failures are known to be influenced by several factors, among which inherited topography plays a key role. Topography, through modifications in the stress and strain fields, can facilitate and/or guide the failure (Ferguson, 1967; Pan *et al.*, 1994, 1995; Savage, 1994; Molnar, 2004; Bois *et al.*, 2012). Savage *et al.* (1985) showed that for symmetric isotropic ridges and valleys gravitational stresses depend on Poisson's ratio as well as on the geometry of the topography: horizontal tensile stresses develop under valleys while compressive stresses exceeding the vertical stress appear near and at ridges. By considering elastic, homogeneous, isotropic self-gravitating models in half-space planes with symmetric ridges or valleys aligned with the regional stresses, Miller and Dunne (1996) showed that stress concentration/diffusion (and thus failure) is influenced by stress orientation. Leith (2012) showed that V-shaped valleys tend to concentrate stresses at their axis or at their ridge crest, depending on the orientation of the tectonic regime. Therefore, it seems that tensile and compressive stress patterns depend on both the regional stress field and Poisson's coefficient.

In terms of slope morphology, it appears that failure occurs between tributary valleys cutting a main slope. An example is the high Tinée valley (Alpes-Maritimes, Southern French Alps). We asked: do tributary valleys, through morphological parameters (lateral spacing and depth) influence slope failure? To tackle this question, we developed numerical models using the FLAC^{3D} code. To validate our assumptions, we considered a realistic 3-D topography model of the La Clapière slope. Then, to test the influence of tributary valley spacing and depth, we examined a second set of models using a simplified 3-D representation of a theoretical Tinée's slope.

Correspondence: Dr. Thomas Bois, Université de Nice Sophia Antipolis, CNRS, IRD, Observatoire de la Cote d'Azur, Géoazur UMR 7329, 250 rue A. Einstein, Valbonne 06560, France. Tel.: +33 6 75 87 17 14; e-mail: thomas.bois@laposte.net

Geological framework

The Tinée valley represents the north-western part of the Argentera-Mercantour massif. The upper valley corresponds to the western boundary between the basement (migmatitic paragneisses covered by a Permo-Triassic tegument) and the detached Mesozoic sedimentary cover (Fig 1). The region underwent a succession of tectonic deformations (Follacci, 1999; Corsini *et al.*, 2004) resulting in (i) a N 150–60°E foliation in the metamorphic basement inherited from the Variscan orogeny (Bogdanoff, 1986; Gunzburger and Laumonier, 2002) and (ii) three sets of tectonic fractures (N 010–30°E, N 080–90°E and N 110–140°E), mainly inherited from the Alpine orogeny, with average dips ranging from 70° to 90° (Fig. 1).

Morphologically, the main slope is cut by several tributary valleys, and movements occur on the slope portions thus delimited (Fig. 2). One of these movements – the La Clapiere landslide, historically active since the beginning of the 20th century (Casson *et al.*, 2005) – has shown dated movements back to ~10 ka (Bigot-Cormier *et al.*, 2005; Sanchez *et al.*, 2010). The landslide is embedded in a larger deformation known as Deep Seated Gravitational Slope Deformation or Sagging (Agliardi *et al.*, 2001; Bois *et al.*, 2008; El'Bedoui *et al.*, 2011) with an upslope propagation (Merrien-Soukatchoff

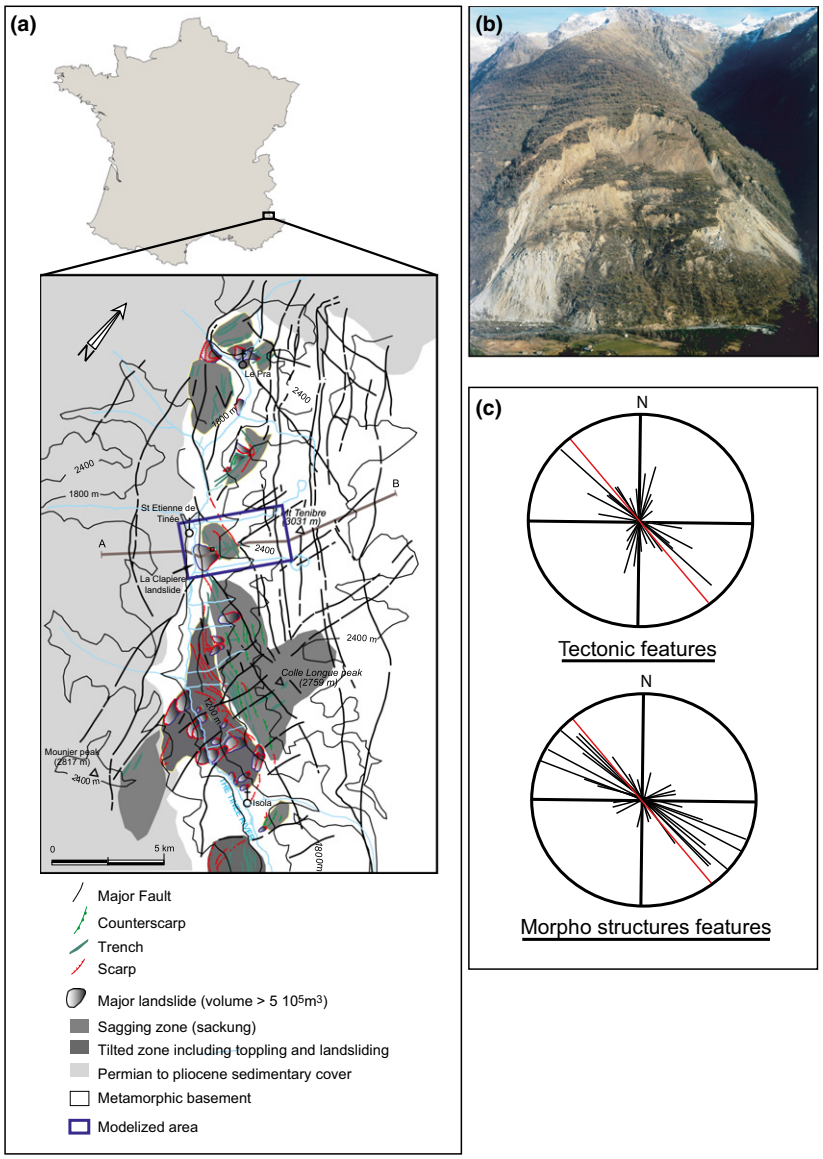

Fig. 1 The Argentera-Mercantour massif and its deformation (modified from Bois *et al.*, 2008). (a) Geostructural context and geomorphological elements in the Argentera-Mercantour massif, and location of the modelled area; (b) La Clapière landslide; (c) Rose diagram of faults and morphostructural features (red lines indicate the orientation of the Tinee Valley).

and Gunzburger, 2005) and a failure surface depth ranging from 100 m to 200 m. The gneissic material in the landslide area is intensively weathered (Guglielmi *et al.*, 2005; Jomard *et al.*, 2007; Lebourg *et al.*, 2012), leading to linear evolutions of both effective cohesion and effective angle of internal friction (respectively decreasing and increasing) from the unweathered area to the weathered area since 3.6 ka (Lebourg *et al.*, 2012).

Numerical modelling

The dynamic finite-difference calculation code FLAC^{3D} was chosen to perform the numerical simulations presented here because of its 'time-marching' explicit solution scheme and because it uses the mixed-discretization zoning technique necessary to ensure accurate modelling of plastic collapse loads and plastic flow (Marti and Cundall, 1982). Deformation was simulated under gravitational loading with roller boundary conditions imposed along the vertical borders. The bottom of the model was either roller or fixed (depending on the tested configuration). The realistic 3-D topography (Figs 3–5) was extracted from a DEM file. In the other cases, a simplified 3-D geometry was used, based on a simplified cross-section (x–z plane, corresponding to the red plane in Fig. 3) of the La Clapière slope extended in the y direction. The first models (Figs 3–5) had a grid zone size of 2.5 × 4.7 km, while other models had a 7 × 7 km grid. Each model had a 1 km extension in the shallow crust and a spatial resolution of 50 m.

The models had homogeneous elastic–plastic properties given by 'Hooke's equation' (1), the Mohr–Coulomb yield function (2) and the plastic potential function (3).

$$d\varepsilon_{ij}^{e} = \frac{d(\frac{1}{3}\sigma_{ii})}{K}\delta_{ij} + \frac{d(\sigma_{ij} - \delta_{ij}(\frac{1}{3}\sigma_{ii}))}{2G} \quad (1)$$

$$f = \sigma_1 - \sigma_3\left(\frac{1+\sin\phi}{1-\sin\phi}\right) - 2C\sqrt{\left(\frac{1+\sin\phi}{1-\sin\phi}\right)} \quad (2)$$

$$\Phi = \sigma_1 - \sigma_3\left(\frac{1+\sin\psi}{1-\sin\psi}\right) - 2C\sqrt{\left(\frac{1+\sin\psi}{1-\sin\psi}\right)} \quad (3)$$

where δ_{ij} is the Kronecker delta; σ_i are the principal stresses: $\sigma_3 \leq \sigma_2 \leq \sigma_1$ (compressive stress is positive); K and G are respectively the elastic bulk and the shear modulii; C is the cohesion; ϕ and ψ are respectively the internal friction and the dilatancy angles; and ε_{ij}^{e} is the elastic strain (ij = 1, 2, 3). During calculation, the inelastic deformation is followed using the effective inelastic shear strain ($\bar{\gamma}^{p}$) because the material damage is proportional to this parameter (Chen and Han, 1988). Models are initially elastically equilibrated under gravity with the parameter values given in Table 1 and derived from the literature (Merrien-Soukatchoff *et al.*, 2001; Willenberg, 2004).

Very few data are available for the ψ values, and we are not aware of such data for gneisses. However, for sedimentary rocks at low mean stress

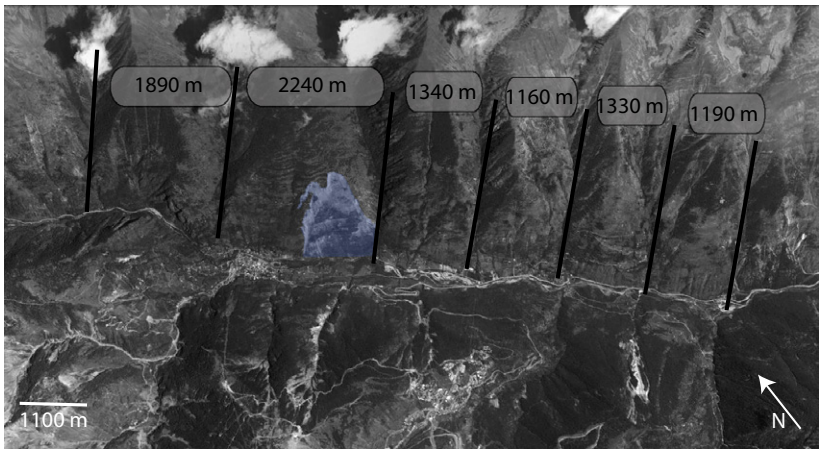

Fig. 2 The high Tinée valley, showing the spacing between tributary valleys (the La Clapière landslide is in blue).

(similar to conditions at the mountain scale), ψ varies from slightly positive to slightly negative (Wong *et al.*, 1997). This justifies the fact that most authors dealing with the mechanical analysis of landsliding assume ψ to be zero or do not take it into account at all (Merrien-Soukatchoff *et al.*, 2001; Ambrosi and Crosta, 2006; Merrien-Soukatchoff and Gunzburger, 2005). Such an assumption was adopted in this study. The initial cohesion value is chosen to ensure that the stress-state is close to the yield surface but still in the elastic domain. While cycling, the value of the cohesion (hereafter C) is incrementally reduced throughout the model. Quasi-static conditions are obtained for a reduction lower than 0.1 C (Chemenda *et al.*, 2009). This can be attributed to the alteration/weathering effects. Indeed, alteration/weathering processes result in a progressive time-softening characterized by a diminution of cohesion (Hill and Rosenbaum, 1998; Hall and André, 2001; Tugrul, 2004; Pellegrino and Prestininzi, 2007; Lebourg *et al.*, 2012). Realistic 3-D topography models were studied with and without *in situ* tectonic stresses. In the La Clapiere slope case, using the 'Hydraulic Tests on Pre-existing Fractures' method (Cornet *et al.*, 1997), we calculated a horizontal to vertical ratio of 0.686. To consider different stress orientations, we extended this to $\sigma_1 > 0.686.\sigma_2 = 0.686.\sigma_3$ (with $\sigma_1 = \sigma_{xx}$ or σ_{yy} or σ_{zz} depending on the case).

Results

3-D models derived from DTM

There are only slight differences in the kinematics of the movements between the tested configurations. At the surface, the deformation is concentrated in two distinct areas: a first one bounded by tributary valleys with its rear part presenting a high $\bar{\gamma}^p$ value, and a second one involving a portion of the right-hand tributary valley exhibiting medium to high $\bar{\gamma}^p$ values. At depth, the deformation ranges from 100 m to 200 m. The higher $\bar{\gamma}^p$ value is reached in the downslope part.

There are differences between the 'roller' (Fig. 3a) and 'fixed' (Fig. 4a) configurations of the model bottom only for the beginning of the deformation pattern. For the fixed bottom condition, the deformation begins in a more diffuse way (compare Figs 3b and 4b). The rest of the pattern (i.e. the failure) is the same (compare Figs 3c and 4c) with comparable $\bar{\gamma}^p$ values (1.5486 and 1.526 respectively for 'roller' and 'fixed' bottom conditions).

Differences in *in situ* stresses (Fig. 5a) again concern only the beginning of the deformation pattern. When the higher *in situ* stress (hereafter $\sigma_{1i.s}$) is in the x–y plane (i.e. $\sigma_{1i.s} = \sigma_{xx}$ or $\sigma_{1i.s} = \sigma_{yy}$), the inelastic deformation is initially concentrated in the valleys perpendicular to the $\sigma_{1i.s}$ direction (compare Fig. 5b, d). When $\sigma_{1i.s} = \sigma_{zz}$, the inelastic deformation is more diffuse, but affects mainly the valleys (Fig. 5f). The rest of the deformation pattern is, once again, almost the same (compare Fig. 5c, e and g) with $\bar{\gamma}^p$ values ranging from 1.5451 ($\sigma_{1i.s} = \sigma_{yy}$) to 2.14 ($\sigma_{1i.s} = \sigma_{zz}$).

These results indicate that: (i) at the time-scale of the process under consideration (landsliding), horizontal displacements due to tectonics and tectonic stresses are not key parameters; and (ii) tributary valleys laterally bound the failure. To determine whether these influences are real, we considered a series of 3-D models with simplified topography.

Simplified 3-D models

Two morphological parameters of tributary valleys were considered: spacing and depth.

Case without tributary valleys (Fig 6a)

Initially, the deformation involves the slope nose, with a maximum depth of ~250 m (Fig. 6b). Through the cycling, the unstable mass keeps sliding down into the valley until the code diverges at $\bar{\gamma}^p$ <1.73 (Fig. 6c).

Case of shallow tributary valleys

Two shallow (i.e. 100 m) tributary valleys were introduced. Their lateral spacing was varied from 500 m to 2500 m. The deformation pattern of the model is the same as in the previous case. For failure, the higher $\bar{\gamma}^p$ values reached are reported in Table 2.

Case of deeper tributary valleys (Fig. 7)

Deeper tributary valleys were introduced (500 m of incision) with a lateral spacing varying from 1000 m (Fig. 7a) to 2000 m (Fig 7d). For spacings between 1000 m and 1300 m (respectively Fig. 7a, b), failure occurs at the sides of the model without involving the central part. The rupture occurs at the sides for $\bar{\gamma}^p$ <0.88246 for 1000 m and 0.88 for 1300 m. Increasing the spacing to 1500 m leads to a different result

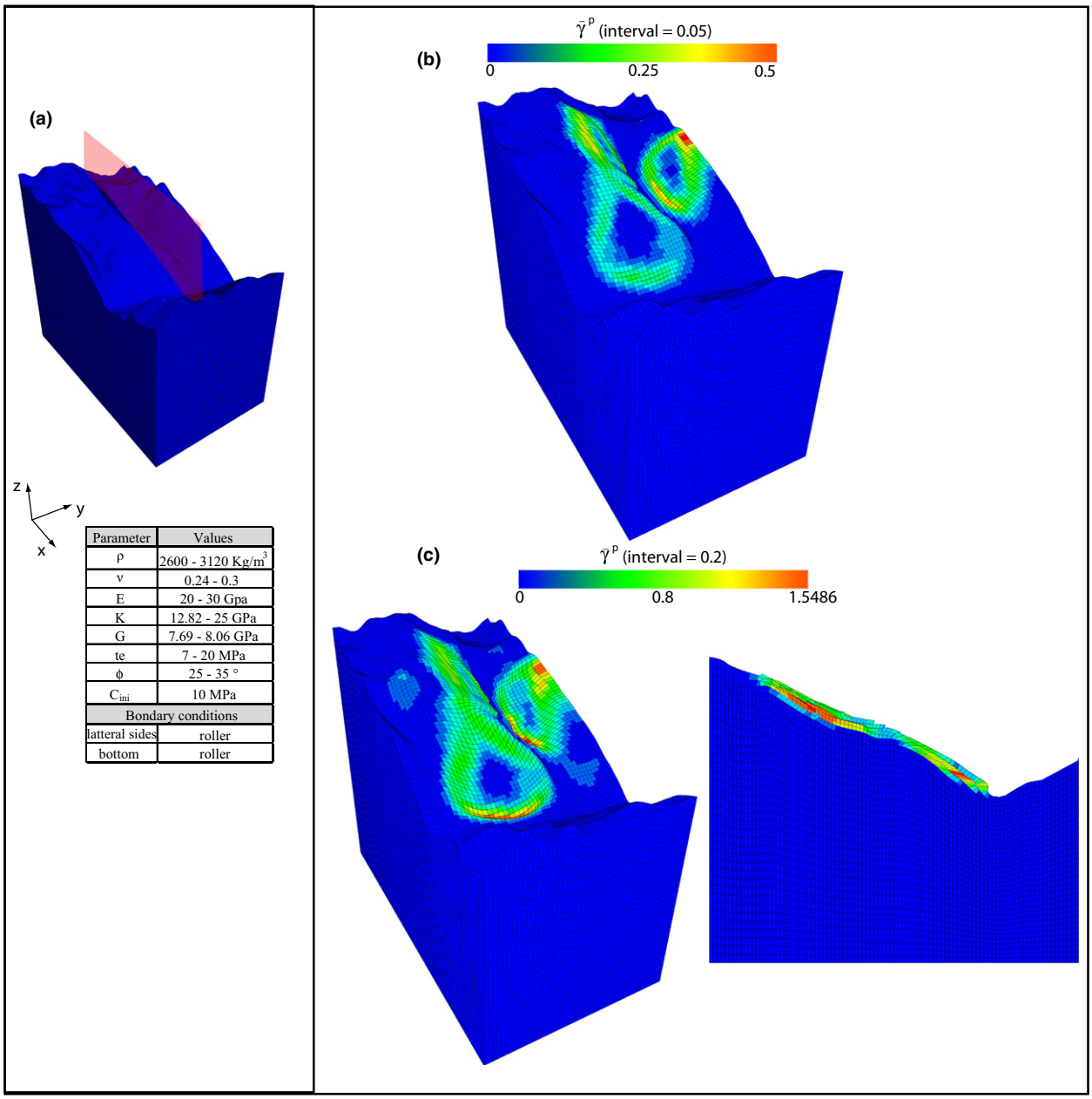

Parameter	Values
ρ	2600 - 3120 Kg/m^3
ν	0.24 - 0.3
E	20 - 30 Gpa
K	12.82 - 25 GPa
G	7.69 - 8.06 GPa
te	7 - 20 MPa
ϕ	25 - 35 °
C_{ini}	10 MPa
Bondary conditions	
latteral sides	roller
bottom	roller

Fig. 3 3-D numerical model of the La Clapière slope with realistic topography under progressive reduction in the cohesion (roller condition at the bottom of the model). (a) Setup. The red plane indicates the orientation of the cross-section; (b) First deformation stage; (c) Final deformation stage (i.e. divergence of the code) and corresponding cross-section.

(Fig. 7c). Failure still occurs at the sides of the model, but now the central part is also involved in the deformation. Nevertheless, rupture still occurs for a $\bar{\gamma}^p$ value of 0.8821. Finally, when the spacing is 2000 m, deformation of the central part of the model occurs (delimiting an unstable mass bounded by tributary valleys). Failure is reached at a $\bar{\gamma}^p$ value of 0.88 (Fig. 7d).

Discussion and Conclusion

To determine the influence of realistic 3-D topography and validate the assumption that tributary valleys bounding a slope can play a role in its gravitational failure, a simple 3-D model was chosen. No inherited structure (e.g. foliation, faults, joints, etc.) was introduced. However, such pre-existing planes of weakness are known to play a role in slope failure, influencing both kinematics and mobilized volumes (Sartori *et al.*, 2003; Bois *et al.*, 2008; Bois and Bouissou, 2010). However, in any modelling approach introducing more than one conditioning factor (e.g. structural heterogeneities and morphological inheritance) is a difficult exercise, and determining (and/or quantifying) the contribution of

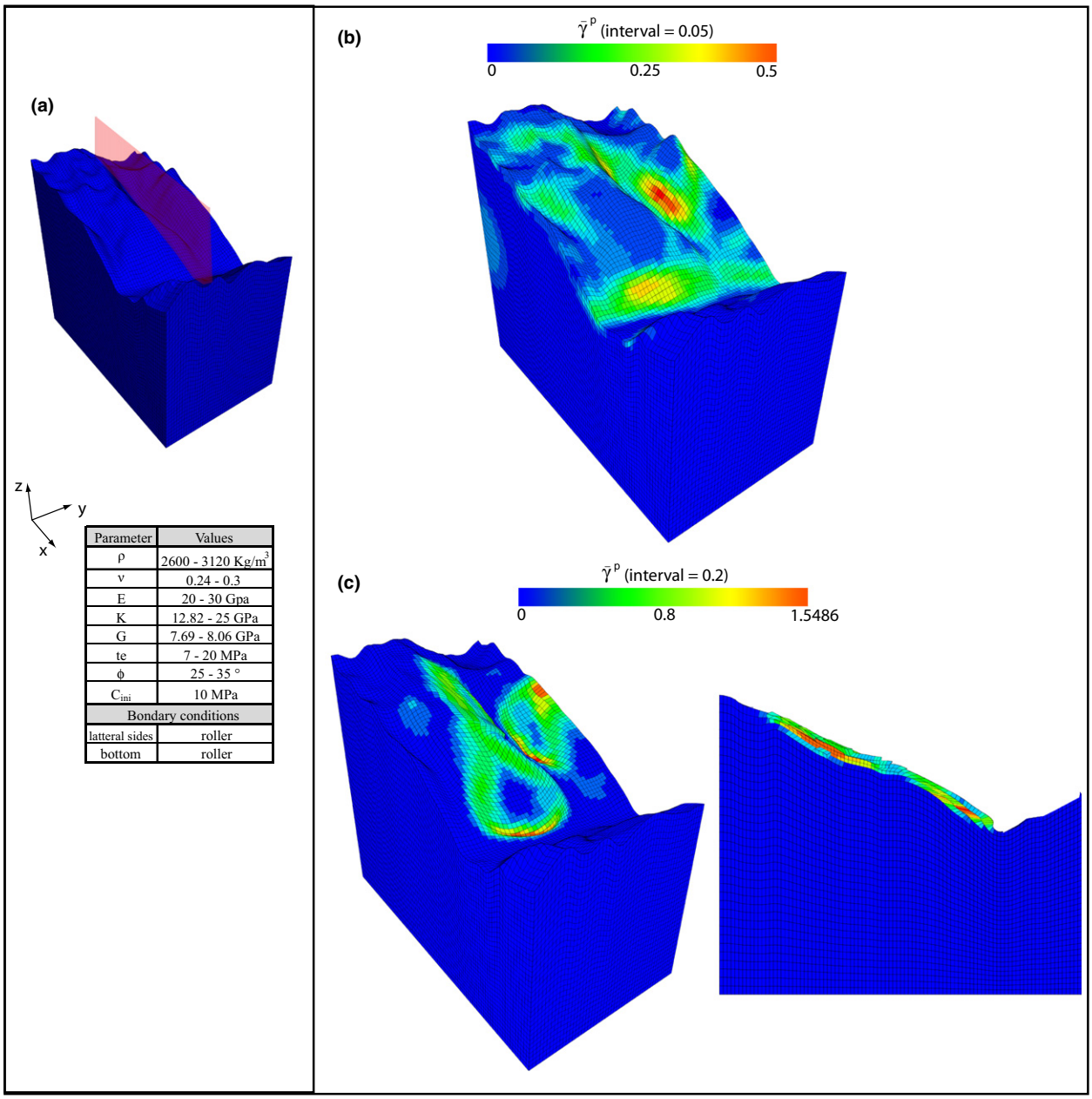

Parameter	Values
ρ	2600 - 3120 Kg/m^3
ν	0.24 - 0.3
E	20 - 30 Gpa
K	12.82 - 25 GPa
G	7.69 - 8.06 GPa
te	7 - 20 MPa
ϕ	25 - 35 °
C_{ini}	10 MPa
Bondary conditions	
latteral sides	roller
bottom	roller

Fig. 4 3-D numerical model of the La Clapière slope with realistic topography under progressive reduction in the cohesion (fixed condition at the bottom of the model). (a) Setup. The red plane indicates the orientation of the cross-section; (b) First deformation stage; (c) Final deformation stage (i.e. divergence of the code) and corresponding cross-section.

each factor is never easy. Here, to be sure of determining only the influence of the morphological parameter under consideration, we used a model with homogeneous elastic-plastic properties, simplifying the natural example. We decided to consider the strength reduction as homogeneous and independent of depth. This assumption can be supported by the fact that strength reduction of a rock mass, mainly due to alteration/weathering effects, is still poorly understood and its variation with depth is not constrained (*i.e.* no rheological law exists on that point). Thus to be sure of not adding an arbitrary depth constraint, strength reduction was not limited with depth.

Roller and fixed bottom boundary conditions have both been used by authors (Merrien-Soukatchoff *et al.*, 2001; Eberhardt *et al.*, 2004; Apuani *et al.*, 2007; Guglielmi and Cappa, 2010). The reality is in between these two cases. We tested models with both types of boundary conditions and, although there were differences at the beginning of the deformation, they are not crucial for this study.

The realistic 3-D topography model provided a good fit to the

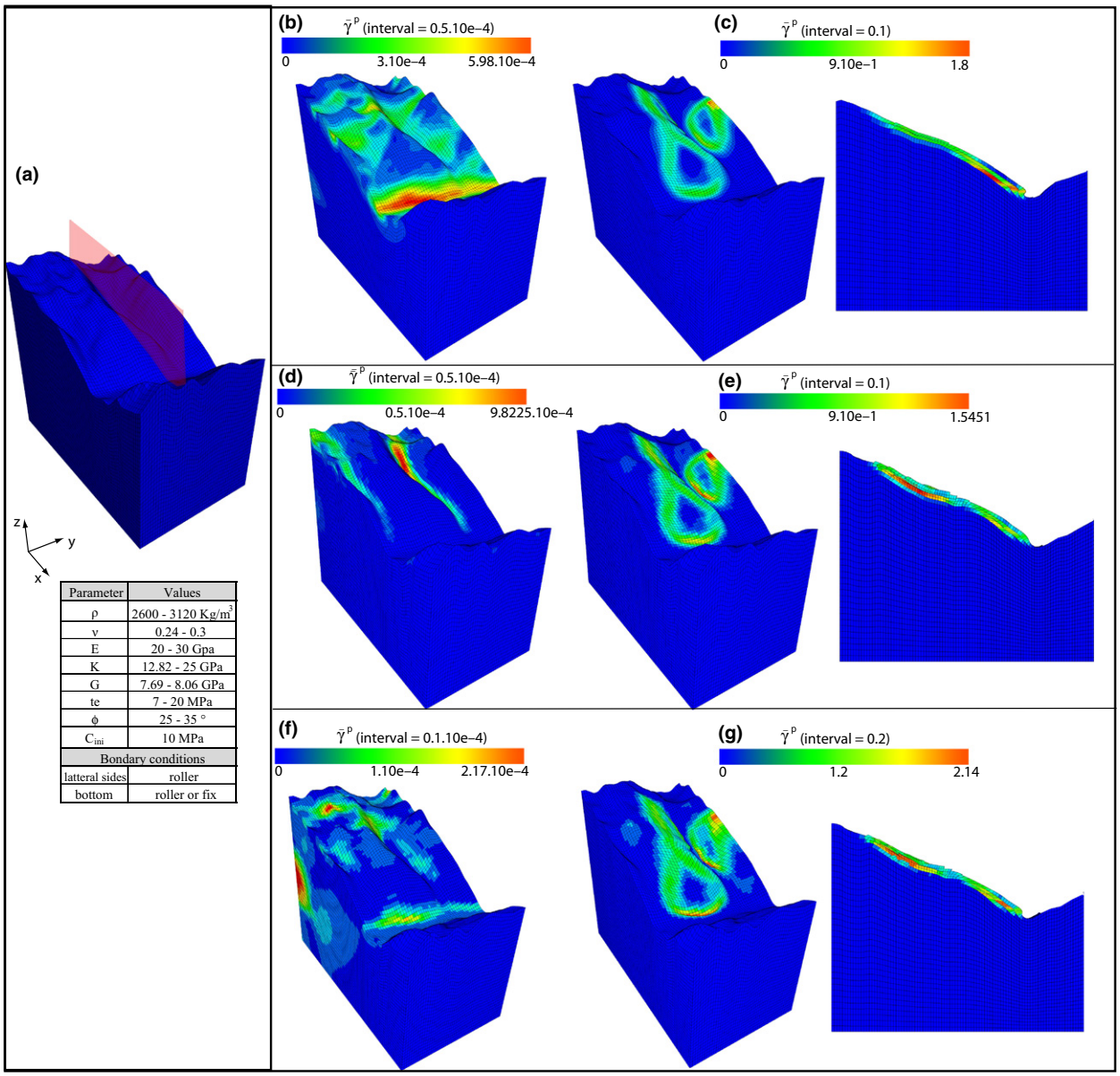

Parameter	Values
ρ	2600 - 3120 Kg/m^3
ν	0.24 - 0.3
E	20 - 30 Gpa
K	12.82 - 25 GPa
G	7.69 - 8.06 GPa
te	7 - 20 MPa
ϕ	25 - 35 °
C_{ini}	10 MPa
Bondary conditions	
latteral sides	roller
bottom	roller or fix

Fig. 5 3-D numerical model of the La Clapière slope with realistic topography under progressive reduction in the cohesion (taking into account *in situ* tectonic stresses). (a) Setup. The red plane indicates the orientation of the cross-section; (b) First deformation stage for *in situ* stresses ($\sigma_1 = \sigma_{xx}$) > ($\sigma_2 = \sigma_{yy}$) = ($\sigma_3 = \sigma_{zz}$); (c) Final deformation stage (i.e. divergence of the code) and corresponding cross-section for *in situ* stresses ($\sigma_1 = \sigma_{xx}$) > ($\sigma_2 = \sigma_{yy}$) = ($\sigma_3 = \sigma_{zz}$); (d) First deformation stage for *in situ* stresses ($\sigma_1 = \sigma_{yy}$) > ($\sigma_2 = \sigma_{xx}$) = ($\sigma_3 = \sigma_{zz}$); (e) Final deformation stage and corresponding cross-section for *in situ* stresses ($\sigma_1 = \sigma_{yy}$) > ($\sigma_2 = \sigma_{xx}$) = ($\sigma_3 = \sigma_{zz}$); (f) First deformation stage for *in situ* stresses ($\sigma_1 = \sigma_{zz}$) > ($\sigma_2 = \sigma_{xx}$) = ($\sigma_3 = \sigma_{yy}$); (g) Final deformation stage and corresponding cross-section for *in situ* stresses ($\sigma_1 = \sigma_{zz}$) > ($\sigma_2 = \sigma_{xx}$) = ($\sigma_3 = \sigma_{yy}$).

natural example considered. Failure was reached in an area compatible with the La Clapière landslide location, with a sliding plane ranging from 100 m to 200 m in depth that propagates from the valley to the upslope as proposed for the La Clapiere landslide (Jomard *et al.*, 2007; Tric *et al.*, 2010). Moreover, the rupture occurs at $C = 0.01$ MPa, which is of the same order of magnitude as the value obtained by Lebourg *et al.* (2012). Comparing our results with those of Chemenda *et al.* (2009) for the same area, failure occurs at a lower $\bar{\gamma}^p$ value in 3-D (1.526 to 2.14 in 3-D vs. $\bar{\gamma}^p = 5.5$ in 2-D), implying that the deformation reached may be overestimated in a 2-D study.

Depending on the orientations of the *in situ* stresses, the inelastic deformation is mainly concentrated in the valleys, while slope failure occurs at the slope toe (with and without *in situ* stresses, whatever their orientation). As proposed by

Table 1 Material properties for the gneissic material.

Parameter	Symbol	Value
Density	ρ	2600–3120 kg m^{-3}
Poisson's ratio	ν	0.24–0.3
Young modulus	E	20–30 GPa
Bulk modulus	K	12.82–25 GPa
Shear modulus	G	7.69–8.06 GPa
Tensile strength	te	7–20 MPa
Friction angle	ϕ	25–35°

Leith (2012), the development of tectonic stresses resulting from both endogenic and exogenic processes strongly influences erosion, forming conduits for water and allowing bedrock incision by water and ice. This implies that *in situ* stresses are key parameters controlling valley shape development, but from our model results, at the time-scale of landsliding, they are not key parameters affecting slope failure.

Tributary valleys also influence the failure process. For shallow incisions, it appears that lateral spacing between tributaries does not affect the localization of the deformation along the slope, but (over the range of investigated spacing) $\bar{\gamma}^p$ values increase with increasing tributary valley spacing, implying an increase in damage (as far as $\bar{\gamma}^p$ is proportional to it), to a stable value of 1.72 (for spacings ranging from 2000 m to 2500 m) comparable with the value obtained without tributary valleys. However, deeper incisions seem to affect slope failure localization but not slope damage, as the $\bar{\gamma}^p$ values obtained in each configuration are similar. In this case, below a certain spacing (1500 m), the effect of one tributary valley on the central part of the slope is offset by the other, so this morphological parameter no longer affects slope failure. Indeed, sliding of the central part occurs for lateral spacings between tributary valleys of more than 1500 m. This shows that

Table 2 $\bar{\gamma}^p$ values reached for lateral spacing of tributary valleys ranging from 500 m to 2500 m (divergence of the code).

Considered lateral spacing	$\bar{\gamma}^p$ value reached (for failure)
500 m	1.62 ± 0.03
1000 m	1.66 ± 0.01
1500 m	1.70 ± 0.01
2000 m	1.71 ± 0.02
2500 m	1.72 ± 0.02

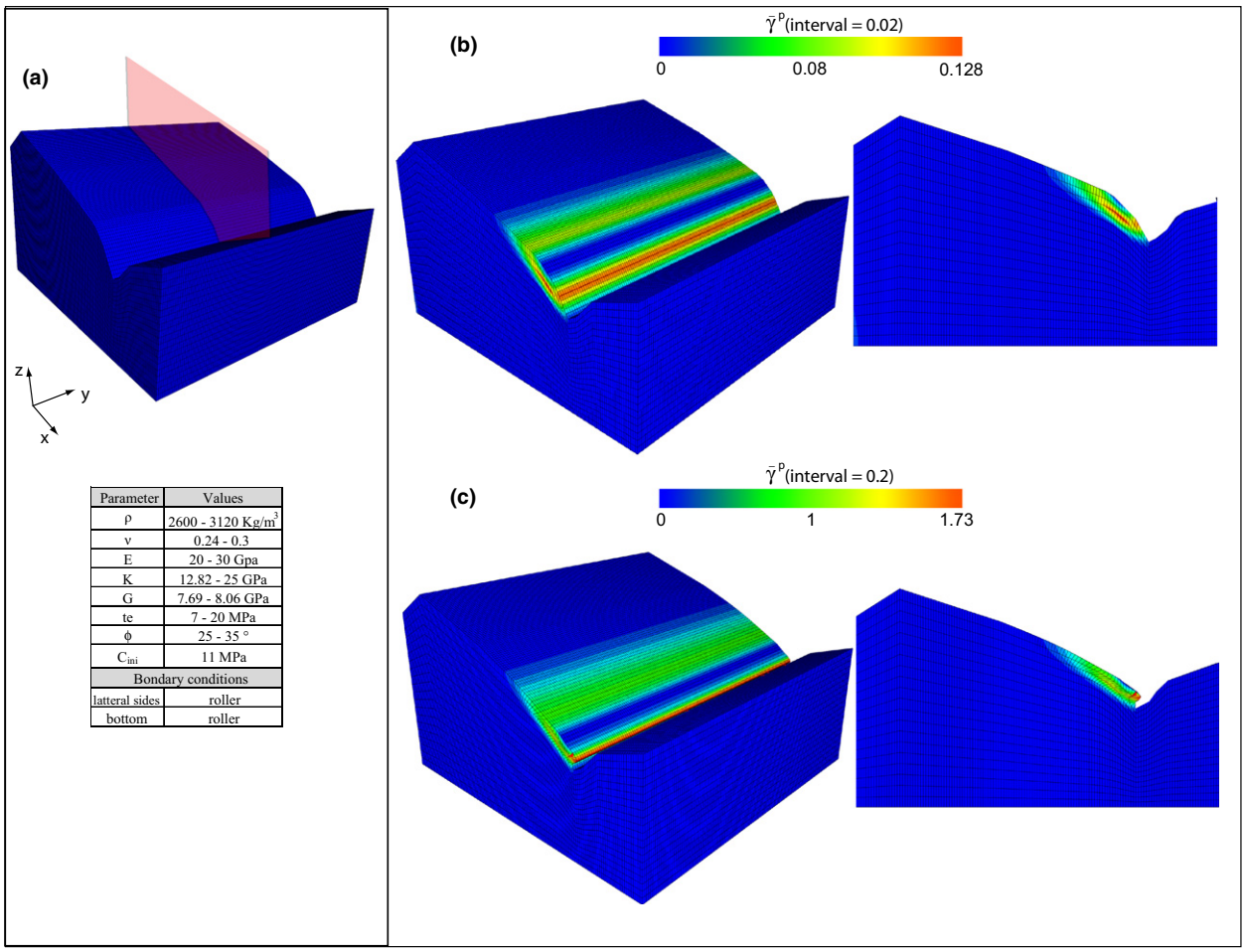

Fig. 6 Evolution of a 3-D simplified model without tributary valleys. (a) Setup. The red plane indicates the orientation of the cross-section; (b) First deformation stage and corresponding cross-section; (c) Last deformation stage (i.e. divergence of the code) and corresponding cross-section.

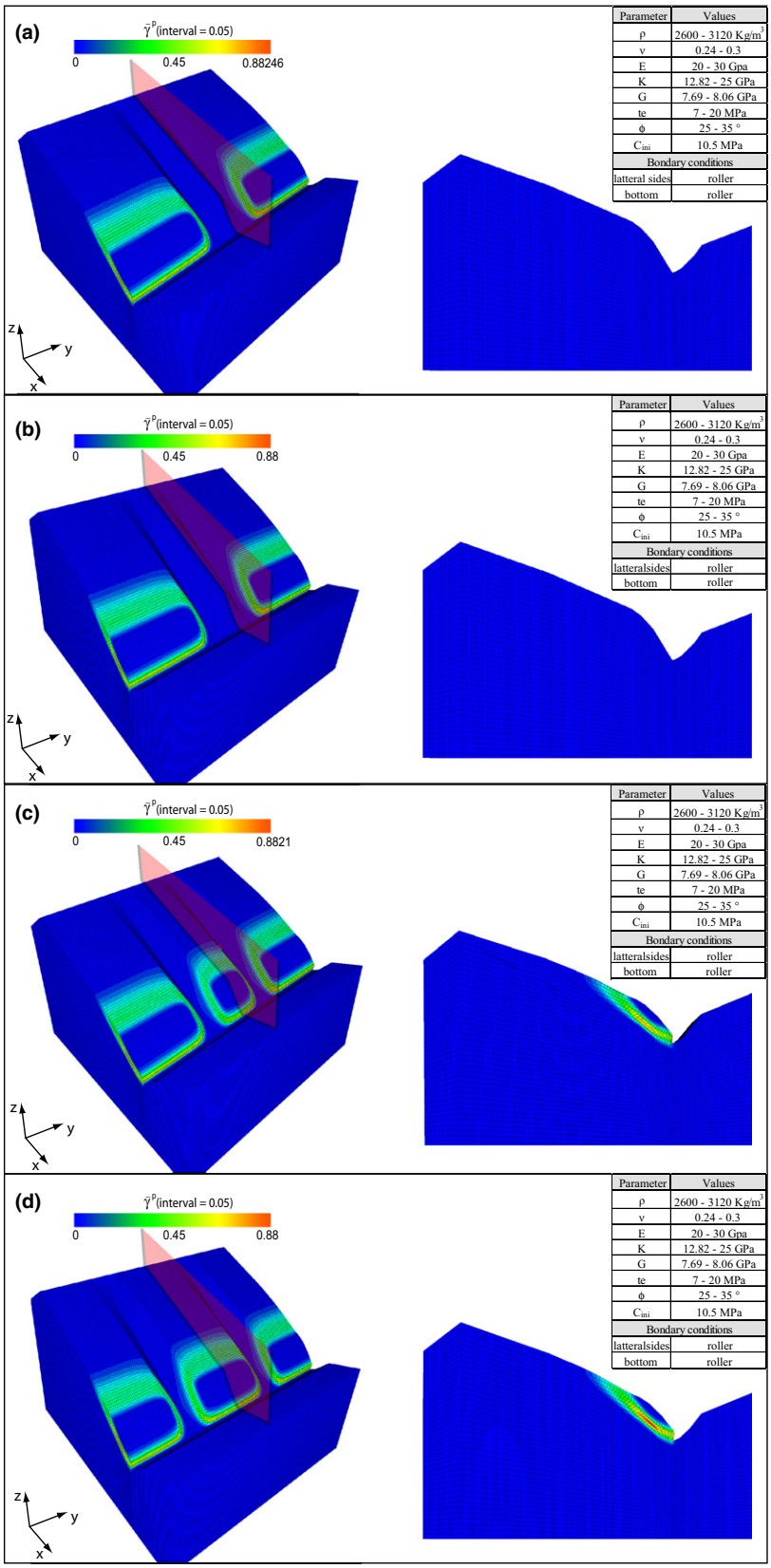

Fig. 7 Evolution of four models with deep tributary valleys (500 m): (a) model with tributary valleys spaced at 1000 m and corresponding cross-section; (b) model with tributary valleys spaced at 1300 m and corresponding cross-section; (c) model with tributary valleys spaced at 1500 m and corresponding cross-section; (d) model with tributary valleys spaced at 2000 m and corresponding cross-section.

for closer spacings the weight of the slope portion laterally bounded by the tributary valleys is not sufficient to initiate a landslide (which can be due to other factors such as tectonic inheritance, weakening, etc.). We conclude that characterizing tributary valleys cutting a slope (through morphologic parameters such as depth and lateral spacing) can be important when studying slope failure.

Acknowledgements

We sincerely thank anonymous reviewers as well as the Associate Editor for their constructive suggestions, criticisms and improving the English.

References

Agliardi, F., Crosta, G. and Zanchib, A., 2001. Structural constraints on deep-seated slopedeformation kinematics. *Eng. Geol.*, **59**, 83–102.

Ambrosi, C. and Crosta, G.B., 2006. Large sackung along major tectonic features in Central Italian Alps. *Eng. Geol.*, **83**, 183–200.

Apuani, T., Masetti, M. and Rossi, M., 2007. Stress-strain-time numerical modelling of a deepseated gravitational slope deformation: preliminary results. *Quatern. Int.*, **171–172**, 80–89.

Bigot-Cormier, F., Braucher, D., Bourlès, D., Guglielmi, Y., Dubar, M. and Stéphan, J.-F., 2005. Chonological constraints on processes leading to large active landslides. *Earth Planet. Sci. Lett.*, **235**, 141–150.

Bogdanoff, S., 1986. Evolution de la partie occidentale du massif cristallin externe de l'Argentera. Place dans l'arc alpin. *Géol. Fr.*, **4**, 433–453.

Bois, T., Bouissou, S. and Guglielmi, Y., 2008. Influence of major inherited faults zones on gravitational slope deformation: a two-dimensional physical modelling of the La Clapière area (Southern FrenchAlps). *Earth Planet. Sci. Lett.*, **272**, 709–719.

Bois, T. and Bouissou, S., 2010. Influence of tectonic fractures zones on

gravitational rock slope failures: New insights from 2-D physical modeling. *J. Geophys. Res.*, **115**, F03009. doi:10.1029/2009JF001403.

Bois, T., Bouissou, S. and Joboyedoff, M., 2012. Influence of structural heterogeneities and of large scale topography on imbricate gravitational rock slope failures: New insights from 3D physical modelling and geomorphological analysis. *Tectonophysics*, **526–529**, 147–156.

Casson, B., Delacourt, C. and Allemand, P., 2005. Contribution of multi-temporal remote sensing images to characterize landslide slip surface – Application to the La Clapière landslide (France). *Nat. Hazards Earth Syst. Sci.*, **5**, 425–437.

Chemenda, A.I., Bois, T., Bouissou, S. and Tric, E., 2009. Numerical modelling of the gravity induced destabilization of a slope: the example of the La Clapière landslide, southern France. *Geomorphology*, **109**, 86–93.

Chen, W.F. and Han, D.J., 1988. *Plasticity for Structural Engineers*. Springer-Verlag, New York.

Cornet, F.H., Wileveau, Y., Bert, B. and Darcy, J., 1997. Complete stress determination with the HTPF tool in mountainous region. *Int. J. Rock Mech. Min. Sci.*, **34**, 3–4.

Corsini, M., Ruffet, G. and Caby, R., 2004. Alpine and late Hercynian geomorphologicalconstraints in the Argentera massif (Western Alps). *Eclogae Geol. Helv.*, **97**, 3–15.

Eberhardt, E., Stead, D. and Coggan, J., 2004. Numerical analysis of initiation and progressive failure in natural rock slopes: the 1991 Randa rockslides. *Int. J. Rock Mech. Min. Sci.*, **41**, 69–87.

El'Bedoui, S., Bois, T., Sanchez, G., Jomard, H., Lebourg, T., Tric, E., Guglielmi, Y., Bouissou, S., Chemenda, A., Rolland, Y. and Perez, J-L., 2011. Paraglacial gravitational deformations in SW Alps: Evidence by field investigations, 10Be cosmogenic dating and physical modelling. *J. Geol. Soc. London*, **351**, 11–25.

Ferguson, H.F., 1967. Valley stress release in the Alleghen Plateau. *Eng. Geol.*, **4**, 63–71.

Follacci, J.P., 1999. Seize ans de surveillance du glissement de La Clapière (Alpes Maritimes). *Bull. Lab. Ponts Chaussées*, **220**, 35–51.

Guglielmi, Y. and Cappa, F., 2010. Regional-scale relief evolution and large landslides: insights from geomechanical analyses in the Tinée Valley (southern French Alps). *Geomorphology*, **117**, 121–129.

Guglielmi, Y., Cappa, F. and Binet, S., 2005. Coupling between hydrogeology and deformation of mountainous rock slopes: insights from La Clapière area (southern Alps, France). *C.R. Geosci.*, **337**, 1154–1163.

Gunzburger, Y. and Laumonier, B., 2002. Origine tectonique du pli supportant le glissement de terrain de la Clapière (NordOuest du massif de l'Argentera–Mercantour, Alpes du Sud, France) d'après l'analyse de la fracturation. *C.R. Geosci.*, **334**, 415–422.

Hall, K. and André, M.F., 2001. New insights into rock weathering from high-frequency rock temperature data: an Antarctic study of weathering by thermal stress. *Geomorphology*, **41**, 23–35.

Hill, S. E. and Rosenbaum, M.S., 1998. Assessing the significant factors in a rock weathering system. *Q. J. Eng. Geol. Hydrogeol.*, **31**, 85–94.

Jomard, H., Lebourg, T., Binet, S., Tric, E. and Hernandez, M., 2007. Characterization of an internal slope movement structure by hydrogeophysical surveying. *Terra Nova*, **19**, 48–57.

Lebourg, T., Hernandez, M., Zerathe, S., Bois, T., Tric, E., Jomard, H. and El Bedoui, S., 2012. Mechanical study and temporal evolution of weathered cataclastic material in gravitational faults of the La Clapière deep-seated landslide, the south-eastern alps. *Landslide*, **8**, 241–252.

Leith, K.J., 2012. Stress development and geomechanical controls on the geomorphic evolution of alpine valleys, PhD. Thesis, University of Canterbury.

Marti, J. and Cundall, P. A., 1982. Mixed Discretization Procedure for Accurate Solution of Plasticity Problems. *Int. J. Numer. Anal. Methods Geomech.*, **6**, 129–139.

Merrien-Soukatchoff, V. and Gunzburger, Y., 2005. Models available to understand failure and pre-failure behaviour of large rock slope movement: the case of "La Clapière", Southern Alps, France. In: *Massive Rock Slope Failure. New models for Hazard Assessment* (S.G. Evans, ed.), *Nato Science Series: IV: Earth and Environmental Sciences*, **49**, 17pp. ISBN 1-4020-4035-0.

Merrien-Soukatchoff, V., Quenot, X. and Guglielmi, Y., 2001. Modélisation par éléments distincts du phénomène de fauchage gravitaire. Application au glissement de La Clapière (Saint – Etienne – de – Tinée, Alpes Maritimes). *Rev. Fr. Géotech.*, **95/96**, 133–142.

Miller, D. J. and Dunne, T., 1996. Topographic perturbations of regional stresses and consequent bedrock fracturing. *J. Geophys. Res.*, **101**, 23–25.

Molnar, P., 2004. Interactions among topographically induced elastic stress, static fatigue and valley incision. *J. Geophys. Res.*, **109**, F02010. doi: 10.1029/2005JF000344.

Pan, E., Amadei, B. and Savage, W.Z., 1994. Gravitational stresses in long symmetric ridges and valleys in anisotropic rock. *Int. J. Rock Mech. Min. Sci. Geomech. Abstr.*, **31**, 293–312.

Pan, E., Amadei, B. and Savage, W.Z., 1995. Gravitational and Tectonic Stresses in Anisotropic Rock with Irregular Topography.. *Int. J. Rock Mech. Min. Sci. Geomech. Abstr.*, **32**, 201–214.

Pellegrino, A. and Prestininzi, A., 2007. Impact of weathering on the geomechanical properties of rocks along thermal-metamorphic contact belts and morpho-evolutionary. *Geomorphology*, **87**, 176–195.

Sanchez, G., Rolland, Y., Corsini, M., Braucher, R., Bourlès, D., Arnold, M. and Aumaître, G., 2010. Relationships between tectonics, slope instability and climate change: Cosmic ray exposure dating of active faults, landslides and glacial surfaces in the SW Alps. *Geomorphology*, **117**, 1–13.

Sartori, M., Baillifard, F., Jaboyedoff, M. and Rouiller, J.-D., 2003. Kinematics of the 1991 Randa rockslides (Valais, Switzerland). *Nat. Hazards Earth Syst. Sci.*, **3**, 423–433.

Savage, W.Z., 1994. Gravity induced stresses in finite slopes. *Int. J. Rock Mech. Min. Sci.*, **31**, 471–483.

Savage, W.Z., Swolfs, H.S. and Powers, P.S., 1985. Gravitational stresses in long symmetric ridges and valleys. *Int. J. Rock Mech. Min. Sci.*, **22**, 291–302.

Tric, E., Lebourg, T., Jomard, H. and Le Cossec, J., 2010. Study of large-scale deformation induced by gravity on the La Clapière landslide (Saint-Etienne de Tinée, France) using numerical and geophysical approaches. *J. Appl. Geophys.*, **70**, 206–215.

Tugrul, A., 2004. The effect of weathering on pore geometry and compressive strength of selected rock types from Turkey. *Eng. Geol.*, **75**, 215–227.

Willenberg, H., 2004. Geologic and kinematics model of a complex landslide in crystalline rock (Randa, Switzerland). Ph.D. Thesis, Swiss Federal Institute of Technology, Zurich.

Wong, T.-F., David, C. and Zhu, W., 1997. The transition from brittle faulting to cataclastic flow in porous sandstones: mechanical deformation. *J. Geophys. Res.*, **102**, 3009–3025.

Received 7 November 2013; revised version accepted 8 March 2014

